PERGAMON

International Journal of Heat and Mass Transfer 42 (1999) 1177–1187

International Journal of HEAT and MASS TRANSFER

Convective heat transfer in the entrance region of a vertical tube for water near the thermodynamic critical point

John R. Howell[a,*], Sang H. Lee[b]

[a] *Department of Mechanical Engineering, The University of Texas at Austin, Austin, TX 78712-1063, U.S.A.*
[b] *Institute of Advanced Engineering, Yongin 449-800, Korea*

Received 20 October 1997; in final form 5 August 1998

Abstract

Turbulent convective heat transfer is modeled for developing flow of water near the thermodynamic critical point in a constant wall temperature vertical tube with and without buoyancy force. Wall temperature effects on momentum and heat transfer, velocity profiles, property variation, heat transfer coefficient, and friction factor distribution close to the inlet ($z/D < 10$) are discussed. Flow acceleration near the wall increases near the critical pressure. Local axial fluid temperature decreases are observed, apparently due to local radial velocity carrying cool core fluid towards the tube wall. Comparison among models for turbulent Prandtl number shows less influence on momentum than heat transfer.

Nomenclature

C_p specific heat at constant pressure [J kg^{-1} K^{-1}]
D tube diameter [m]
f friction factor $= 8\tau_w/(\rho_b u_b^2)$
g acceleration due to gravity [m s^{-2}]
G mass flux [kg m^{-2} s^{-1}]
Gr_L Grashof number $= \rho_b g L^3 |\rho_b - \rho_w|/\mu_b^2$
h heat transfer coefficient [W m^{-2} K^{-1}]
i enthalpy [J kg^{-1}]
k thermal conductivity [W m^{-1} K^{-1}]
K non-dimensional compressibility
l_m mixing length [m]
L tube length [m]
P pressure [Pa]
Pr Prandtl number $= \mu C_p/k$
P_R reduced pressure $= P/P_c$
Q heat flux [W m^{-2}]
r radial coordinate [m]
R radius of tube [m]
Re Reynolds number $= GD/\mu$
Re_L Reynolds number $= (L/D)\,Re$
T temperature [K]
u velocity in axial direction [m s^{-1}]
v velocity in radial direction [m s^{-1}]
y radial distance from the wall [m]
y^* non-dimensional radial distance from the wall $= 1-(r/R)$
y^+ dimensionless distance from the wall $= y\sqrt{\rho\tau_w/\mu^2}$
z axial coordinate [m].

Greek symbols
α grid non-uniformity parameter
β compressibility [K^{-1}]
ε turbulent diffusivity [m^2 s^{-1}]
θ non-dimensional temperature $= (T-T_{in})/(T_W-T_{in})$
μ absolute viscosity [kg s^{-1} m^{-1}]
ρ density [kg m^{-3}]
τ shear stress [N m^{-2}]
ϕ function variable.

Superscripts and subscripts
b bulk condition
c critical point value
H heat
i iteration
in inlet condition
M momentum
pc pseudocritical point
t turbulent flow

* Corresponding author. Fax: 001 512 471 1045; e-mail: jhowell@mail.utexas.edu

0017–9310/98/$ - see front matter
PII: S0017–9310(98)00263–4

w wall condition
* property ratio with inlet value.

1. Introduction

Above but near the thermodynamic critical point, thermodynamic and transport variables show anomalous characteristics. A graph of temperature vs. entropy near the critical point for water is shown in Fig. 1 for various pressures. Entropy increases with an increase of temperature, and as pressure approaches the critical pressure the gradient becomes steeper.

For fluids near the critical point, the characteristics of heat and momentum transfer are complicated by the large variation in density, specific heat, viscosity, and thermal conductivity with pressure and temperature. When the temperature of the fluid is near the pseudocritical point, phase transition-like phenomena occur across the steep property variations that occur between liquid-like and gas-like behavior. There is a peak in specific heat and thermal conductivity at this boundary-like temperature. The peak in viscosity is much smaller and is usually neglected. Specific heat has a more pronounced peak than thermal conductivity, and both of these peaks increase very rapidly as the pressure approaches the critical value.

Figure 2 shows the density variation of water in the critical region for several pressures. Density decreases with increasing temperature and the variation becomes steeper as the pressure approaches the critical point ($T_c = 647.07$ K, $P_c = 22.05$ MPa). The density at the pseudocritical temperature increases very slowly with increasing pressure. Above 30 MPa, the variation is smooth although specific heat still has a non-negligible peak at the pseudocritical temperature. The pseudocritical temperature at which there is a large peak increases with increasing pressure. The near-linear relationship between pseudocritical temperature and pressure is shown in Fig. 3 from an interpolation equation in the range of $1 < P_R < 1.5$.

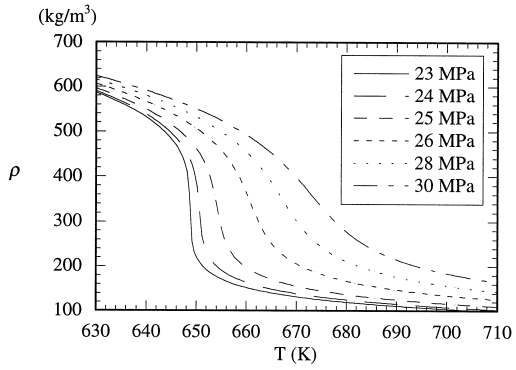

Fig. 2. Water density variation with temperature for several pressures near the critical point.

Fundamentally, the variations in properties are coupled with momentum and heat transfer characteristics in the fluid flow through the thermodynamic state variables of temperature and pressure. The highly non-linear variation in these properties makes flow phenomena more unpredictable compared with the constant property case.

A large amount of experimental and theoretical research has been carried out to study heat transfer phenomena near the critical point in a tube because of applications in power generation systems, rockets, and superconductor systems. Before the mid 1970s, research provided experimental data, correlations for the heat transfer coefficient, and theoretical analyses for use in design [1–6]. Investigators tried to understand the physical phenomena and understand the difference between the results for constant properties and variable properties near the critical point. The suggested correlations for heat transfer coefficient included additional parameters

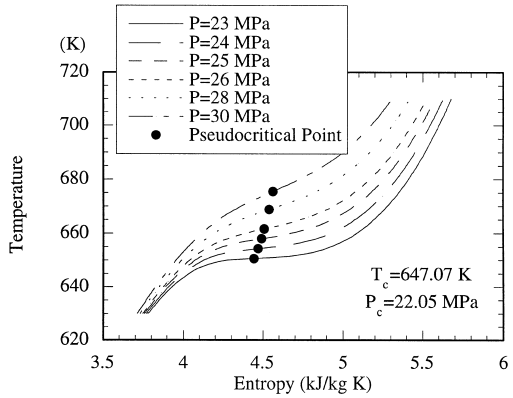

Fig. 1. Temperature–entropy chart for water near critical point.

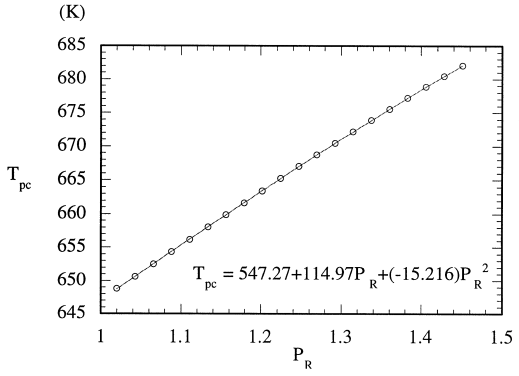

Fig. 3. Variation of pseudocritical temperature with reduced pressure for water.

or changes in the coefficients of the constant-property-based equations to account for the effect of property variations. However these correlations are not consistent. They produce poor predictions if the fluid is changed or variable ranges of the original data used for the correlation are exceeded.

Some studies [2] suggested that heat transfer characteristics near the critical region resemble boiling because of the steep variation of properties between liquid-like behavior and gas-like behavior. The theoretical models tried to describe the heat transfer phenomena by including a phase related parameter, but some later research rejects this model because a supercritical fluid in equilibrium is truly single phase, but the pseudoboiling model assumes it is not. Visual studies [5] of the flow field do not detect bubble-like phenomena near the critical region.

Since the 1970s, some experimenters have measured the heat transfer coefficient and wall temperature distribution along a uniformly heated tube [7–12]. They aimed to explain the phenomenon of deterioration of heat transfer coefficient for turbulent flow in a vertical tube, which is related to steep property variations. They also tried to find the parameter values that provide improved heat transfer near the pseudocritical temperature. With the development of computers, numerical analyses [13–21] can predict heat and momentum transfer by solving the coupled governing conservation equations simultaneously with property variations. They show the effect of properties on convection heat transfer and the heat transfer coefficient distribution along the tube. A large heat transfer coefficient is predicted when the fluid temperature is near the pseudocritical temperature. Gravity has an important influence on heat transfer in a vertical tube because of the steep variations in density near the pseudocritical point. This influence is a factor in the observed local deterioration in the heat transfer coefficient. Most of the predictions are qualitatively in accord with experimental results but quantitatively there are some differences. The predictions for turbulent flow are usually based on the mixing length or κ–ε models, and some have introduced modifications in modeling compared with standard constant-properties models [14, 15]. These models are intended to investigate temperature and velocity distributions along the tube as well as heat transfer coefficient and wall temperature distributions. However, because of the lack of experimental data inside the flow field, it is difficult to verify the predicted flow and heat transfer phenomena. Many predictions for turbulent flow are obtained with a constant-property-based model so property variation effects on thee models are still not well understood.

In previous work, we investigated convective transfer at near-critical-point conditions for fluids in laminar flow with and without the effect of a gravitational field [20, 21], and we examined turbulent flow in a vertical tube using a mixing-length model including comparisons with existing experimental data [23].

In this study, convection heat transfer phenomena in the entrance region of a vertical tube for water near the critical point is predicted by numerical simulation in order to understand momentum and heat transport inside the tube with property variations. A two-dimensional model to solve the governing conservation equations of motion and energy is established and numerically solved. The model includes the effect of thermodynamic and transport properties. In order to understand the effect of the property variations on turbulent Prandtl number in modeling of turbulent flow of near-critical fluids, several models are applied and the predicted results are compared. This helps to predict and understand the momentum and heat transfer in the entrance region of a tube for fluids near their critical point.

2. Numerical modeling

For flow in a vertical tube, momentum and heat transfer are described by the two-dimension conservation equations. Flow is assumed to be axisymmetric and steady state, and the tube is smooth. For thermodynamic and transport properties, water is assumed to be in local thermodynamic equilibrium. The governing conservation equations of continuity, momentum, and energy are:

Continuity

$$\nabla\cdot\overline{\rho V}=0. \tag{1}$$

Momentum

$$\nabla\cdot\overline{\rho VV}=-\nabla P+\overline{\nabla\cdot\tau}+\rho g. \tag{2}$$

Energy

$$\nabla\cdot\overline{\rho Vi}=\nabla\cdot\left[\left(\frac{\mu}{Pr}+\frac{\mu_t}{Pr_t}\right)\nabla i\right]-\nabla\cdot\left\{\left[\frac{(1-\beta T)k}{\rho C_p}\right]\nabla P\right\}+\frac{DP}{Dt}+\mu\bar{\Phi} \tag{3}$$

where $\bar{\Phi}$ is viscous dissipation. All properties of water are calculated at the local temperature and pressure in the flow field.

The mixing length model suggested by Bellmore and Reid [14] is used in this study for the calculation of turbulent transport. The turbulent viscosity is expressed in this model as

$$\mu_t=\rho l_m^2\left|\frac{\partial u}{\partial y}\right|\left[1-\left(\frac{\beta}{C_p}\frac{l_m}{Pr_t}\frac{\partial i}{\partial y}\right)-\left(\frac{\beta}{C_p}\frac{l_m}{Pr_t}\frac{\partial i}{\partial y}\right)^2\right]. \tag{4}$$

This modified form of the mixing length model includes the effect of density fluctuations on turbulent transport. A typical two layer model is used for mixing length calculations. The turbulent Prandtl number $\varepsilon_M/\varepsilon_H$ is assumed to be 0.9 in most of the calculations [16, 18, 19] and three other models of turbulent Prandtl number are used in several cases to see the effect of turbulent Prandtl number on the heat transfer. These models are

1. Reynolds analogy

$$Pr_t = 1.0. \tag{5}$$

2. Kays and Crawford [23]

$$Pr_t = \frac{1}{\left\{\frac{1}{1.7} + (0.3Pe_t)\sqrt{\frac{1}{0.85}} - (0.3Pe_t)^2 \times \left[1 - \exp\left(-\frac{1}{\sqrt{0.85}(0.3Pe_t)}\right)\right]\right\}}. \tag{6}$$

3. Kays [24]

$$Pr_t = 2.0/Pe_t + 0.85 \tag{7}$$

where

$$Pe_t = (\mu_t/\mu)Pr. \tag{8}$$

As flow boundary conditions, uniform radial inlet velocity and temperature are assumed. Constant temperature is applied at the tube wall and the symmetry condition is used at the centerline of the tube. At the exit boundary of the tube, the dependent variables are extrapolated linearly to provide the axial downstream conditions.

In this study most cases considered have inlet fluid temperature below both the pseudocritical temperature at the specified inlet pressure and the critical temperature, which are in turn lower than the wall temperature. Hence there is large variation in the properties between the wall and centerline of the tube. All thermodynamic and transport properties for water are calculated with the program of Lester et al. [25]. If there is any recirculation due to large buoyancy force near the wall, this model is not appropriate. Hence any case with flow recirculation in the tube is not considered in this study. If the tube is long enough, recirculation will occur and the flow will have complicated unsteady characteristics, and will also probably be three-dimensional.

3. Solution procedure

Equations (1)–(3) are solved numerically by the finite difference control volume method, SIMPLE procedure [26] with the appropriate boundary conditions. The converged solution is obtained when the following convergence criteria are satisfied for the dependent variables.

$$\left|\frac{\phi^{i+1} - \phi^i}{\phi^i}\right| < 10^{-3}; \quad \phi = u, v, \quad \text{and} \quad i. \tag{9}$$

This calculation is for low Reynolds number turbulence modeling because the effect of property variation cannot be neglected near the wall and it is not possible to apply the wall function in that region [19]. Hence the grid must be very fine near the wall in order to apply Couette flow in the laminar sublayer ($y^+ = y\sqrt{\rho\tau_w/\mu^2} < 5$). For this calculation an axially and radially non-uniform orthogonal grid system is used. The following relations [27] are used in the radial and axial grid system,

$$r = \frac{(\alpha_r + 1) - (\alpha_r - 1)\{[(\alpha_r + 1)/(\alpha_r - 1)]^{1-\bar{r}}\}}{[(\alpha_r + 1)/(\alpha_r - 1)]^{1-\bar{r}} + 1} \tag{10}$$

$$z = \frac{(\alpha_z + 1) - (\alpha_z - 1)\{[(\alpha_z + 1)/(\alpha_z - 1)]^{1-\bar{z}}\}}{[(\alpha_z + 1)/(\alpha_z - 1)]^{1-\bar{z}} + 1} \tag{11}$$

where $\bar{r}$, $\bar{z}$ is the uniformly distributed grid system. This system clusters the grid in the region near the entrance and near the tube wall as α_r and α_z approach unity.

For the most calculations with $L/D = 10$, a grid of 200×100 (axial $\times$ radial) is used. Grid dependence of the solution was checked by refining the radial and axial grid system. The values of non-uniformity parameters, α_r and α_z are 1.001 and 1.5, respectively, to give enough grid points near the wall and entrance of the tube where there are large variations in flow and heat transfer variables. The effect of the extrapolation boundary condition at the exit of the tube was checked by increasing the L/D to larger values and checking for changes at upstream locations.

4. Results and discussion

4.1. Comparison with other modeling

To verify the results from our model, we compared them with the numerical results of Zhou and Krishnan (1995) [19]. The geometry considered is a two-dimensional symmetric channel flow with gravity in the developing region. The supercritical fluid considered by Zhou and Krishnan is carbon dioxide and its local properties are calculated [28] (all other results shown in this paper are for water). Figure 4 shows comparison of velocity, temperature, and density distributions inside the channel. With heat transfer from the wall at constant heat flux, the fluid temperature increases beyond the pseudocritical temperature near the wall and there is a flow acceleration near the wall due to buoyancy force. It can be seen that the two predictions agree well. We earlier compared our numerical model to experimental results [22].

We now proceed to the vertical tube geometry using water as the working fluid for conditions near the thermodynamic critical point.

4.2. Effect of pressure on buoyancy force

At pressures near the critical pressure ($P_c = 22.05$ MPa), water near the constant-temperature hot wall in the vertical tube accelerates in the axial direction and incurs a steep velocity gradient. This is due to the increase of the buoyancy force, which results from the density

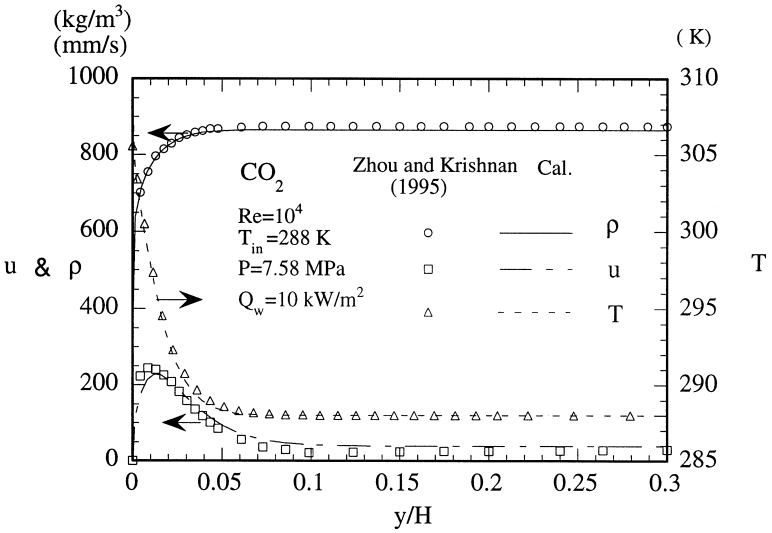

Fig. 4. Comparison of this modeling prediction with [19] for velocity, temperature, and density distributions in a channel for upward flow of CO_2.

difference between the wall and bulk fluid (inlet) temperature (Fig. 2). A bulk buoyancy force parameter for the entrance region and high velocity considering boundary layer development, Gr_L/Re_L^2 can be represented as

$$\frac{Gr_L}{Re_L^2} = \frac{\rho b g \Delta L}{G^2} \approx \frac{\rho_{in} g \Delta \rho L}{G^2} \tag{12}$$

where the density difference is

$$\Delta\rho = (\rho_w - \rho_b) \approx (\rho_w - \rho_{in}). \tag{13}$$

This buoyancy force parameter considers density differences between the bulk fluid and the fluid at the wall. As can be seen in equations (12) and (13), density difference and mass flow rate are the most important parameters in the buoyancy force. Since density variation near the pseudocritical point is locally very steep, it should be considered as another parameter affecting the buoyancy force when the pseudocritical temperature is between the wall and bulk temperatures. Although the region with steep density variation is very narrow and close to the wall, it can generate a large buoyancy force which results in flow acceleration as well as heat transfer enhancement. The maximum non-dimensional density gradient with temperature in a cross section of the tube is

$$K = \left|\frac{\rho\beta\Delta T}{\Delta\rho}\right|_{max} = \left|\frac{\rho\beta(T_w - T_{in})}{(\rho_w - \rho_{in})}\right|_{max}. \tag{14}$$

Figure 5 shows the effect of pressure on the buoyancy parameter of equation (12) and the density gradient for constant inlet and wall temperatures. As the pressure increases, the effect of buoyancy force decreases because of the decrease in the density variation with temperature. The buoyancy parameter of equation (12) for $P_R = 1.020$ is about two times that for $P_R = 1.361$. The parameter for $P_R = 1.361$ is about 9.6 and, from an order of magnitude analysis, free convection effects on fluid flow and heat transfer still cannot be neglected.

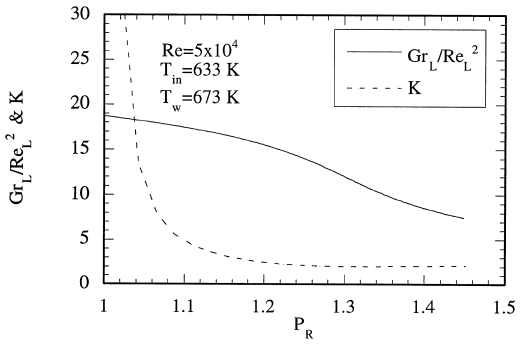

Fig. 5. Variation of buoyancy force parameters with pressure for water.

Higher acceleration near the wall results in an increase of heat transfer coefficient. The temperature which has the maximum density gradient is a little lower than the pseudocritical temperature and the temperature difference increases as the pressure increases. It increases very steeply as the pressure approaches the critical point compared with the buoyancy parameter of equation (12). Axially and radially the pressure drop in the tube is very small because of small L/D being considered, so the effect of pressure on property variations in the tube is negligible compared with that of temperature,

Distributions of axial velocity and thermodynamic

properties (e.g., density and specific heat) of water inside a vertical tube for two pressures are shown in Figs 6 and 7. With higher buoyancy effect due to larger density variation between the wall and bulk fluid as well as lower viscosity, the fluid near the wall is accelerated more at 24 MPa than at 28 MPa. There are steep variations in fluid properties in a narrow region close to the wall. The specific heat of water is larger at 24 MPa, with a more pronounced peak value. Because of the higher pseudocritical temperature at 28 MPa, the location of the peak in specific heat (and thus fluid enthalpy) is closer to the wall. This combination of high acceleration of the fluid and large specific heat act to increase the turbulent transport. This improves the heat transfer even though the thermal conductivity of fluid at the wall is low. Hence, both the fluid density and specific heat (enthalpy) increase faster at 24 MPa between the two axial positions ($z/D = 1.0$ and 4.0) due to this higher heat transfer, which is reflected in a greater fluid temperature increase.

Heat transfer coefficient distributions along the tube for various pressures with or without the effect of the gravity force term are shown in Fig. 8. The heat transfer coefficient, h is shown rather than Nusselt number, because the value of thermal conductivity varies with

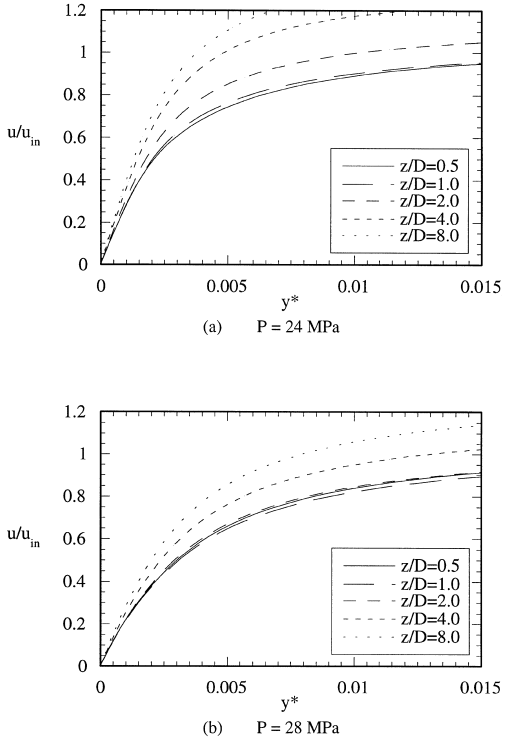

Fig. 6. Comparison of predicted velocity distributions in a tube for upward flow of water; $Re = 5 \times 10^4$, $T_{in} = 633$ K, $T_w = 673$ K.

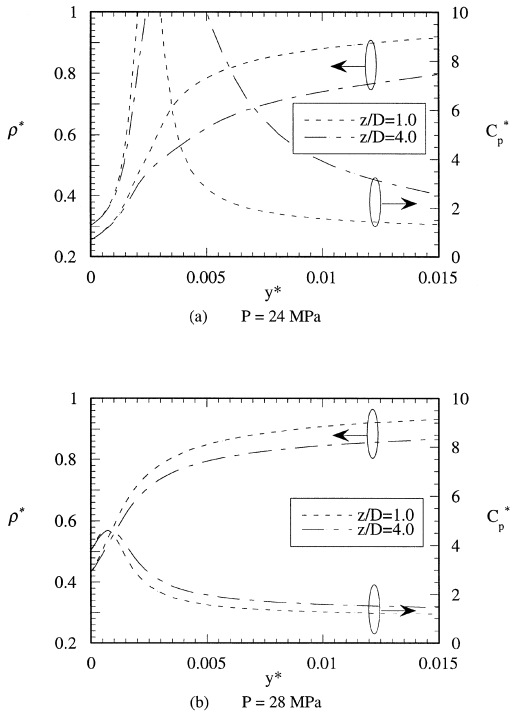

Fig. 7. Comparison of predicted density and specific heat distributions in a tube for upward flow of water; $Re = 5 \times 10^4$, $T_{in} = 633$ K, $T_w = 673$ K.

inlet pressure and thus obscures understanding of the Nu variation. Near the entrance of the tube ($z/D < 0.5$) for upward flow the heat transfer coefficient decreases very rapidly. In this region there is not much difference in the heat transfer coefficients at different pressures. Heat transfer coefficients at larger z/D start to increase due to the buoyancy effect, and the starting location of the increase along the tube moves closer to the entrance as the pressure approaches the critical pressure ($z/D = 1.5$ for $P = 25$ MPa and $z/D = 5.5$ for $P = 30$ MPa). Although the tube region considered is short, at $z/D = 5.0$ the heat transfer coefficient for $P = 25$ MPa is about 25% higher than for $P = 30$ MPa. From this location, the heat transfer coefficient increases almost linearly along the tube, and the difference in the heat transfer coefficients for various pressures also increases along the tube.

For flow neglecting the gravity force term, there is less variation in the heat transfer coefficient distributions as the pressure in the tube changes. Close to the entrance of the tube, ($z/D < 6$), the heat transfer coefficient increases with increasing pressure due to the fluid thermal conductivity increase at the wall. Downstream, ($z/D > 6$), the heat transfer coefficient increases with the pressure because the effects of both bulk fluid acceleration (due to

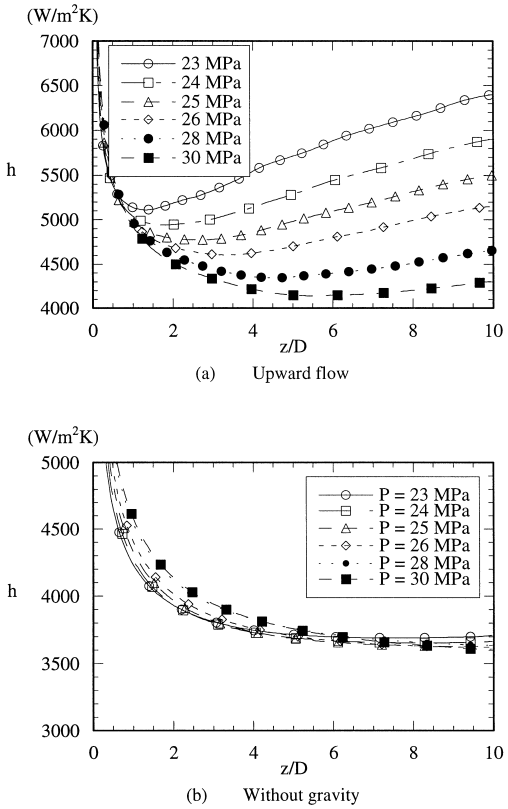

Fig. 8. Heat transfer coefficient distributions along a tube in upward and without-gravity flow of water for various pressures; $Re = 5\times10^4$, $T_{in} = 633$ K, $T_w = 673$ K.

density decrease) and increasing turbulent transport (with increased specific heat) become more important. Comparison of the results with and without gravity shows that buoyancy force due to density variation has an important effect on heat transfer in the tube compared with other property variations and its effect becomes even more important as the flow rate decreases. Because of the non-linear variation of thermodynamic and transport properties with pressure and temperature for near critical fluids, momentum and heat transfer are coupled through the properties. It is difficult, therefore, to find a relation between heat transfer coefficient and the buoyancy force parameter as suggested by equation (12).

4.3. Wall temperature effect

The buoyancy force depends on temperature level and wall–fluid temperature difference as well as pressure. Because of the non-linear variation of properties with temperature near the pseudocritical temperature for a specified pressure (Fig. 2), the usual Boussinesque approximations [23] cannot be applied. In particular, the density gradient with temperature (compressibility) is high at the pseudocritical temperature, and as the pressure increases the gradient at the pseudocritical temperature decreases. The buoyancy force thus depends on the magnitude of temperature and pressure in addition to the temperature difference. Table 1 shows the values of the buoyancy force parameter, Gr_L/Re_L^2 for several wall temperatures with thermal conductivities and dynamic viscosities evaluated at the wall temperatures. All of the buoyancy force parameter values are larger than unity so buoyancy effects cannot be neglected in the entrance region at these conditions regardless of Reynolds number. The parameter values at wall temperatures equal to the pseudocritical temperature, T_{pc} and 673 K are about five and eight times higher than at 643 K.

The Grashof number variation with wall temperature is non-linear due to the dependence of the thermophysical properties on temperature. Although density difference is the main driving force for buoyancy, other property variations cannot be neglected because fluid flow and heat transfer are coupled through the thermodynamic and transport properties.

The distributions of heat transfer coefficient for various wall temperatures are shown in Fig. 9. When the wall temperature is 643 K, the heat transfer coefficient decreases almost continuously along the tube. As the wall temperature increases above the pseudocritical temperature, the heat transfer coefficient goes through a minimum near the entrance of the tube. As the wall temperature increases past the pseudocritical temperature, the thermal conductivity at the wall decreases, then increases a little near the pseudocritical temperature, and then decreases again. The thermal conductivities at the pseudocritical temperature, T_{pc}, and at 673 K are about 2 and 64% lower than the values at 643 K. Because of the high flow velocity and short length of the tube, ($L/D = 10$), the increase of the bulk fluid temperature is small compared with the temperature difference between

Table 1
Buoyancy force parameter dependence on the wall temperature with transport properties at the wall for water; $Re = 5\times10^4$, $P = 24$ MPa, $T_{in} = 633$ K

T_w (K)	Gr_L/Re_L^2	k_w^* ($=k_w/k_{in}$)	μ_w^* ($=k_w/k_{in}$)
643	2.210	0.934	0.904
648	3.976	0.896	0.831
653	8.062	0.913	0.675
T_{pc} ($=654$)	10.71	0.917	0.583
658	14.96	0.559	0.463
663	16.41	0.426	0.434
673	17.63	0.331	0.418
683	18.28	0.290	0.414

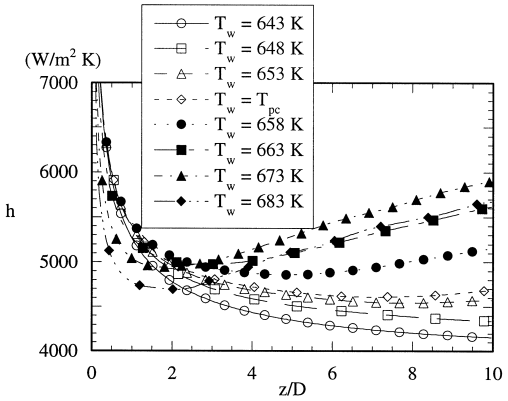

Fig. 9. Heat transfer coefficient distributions along a tube in upward flow of water for various wall temperatures; $Re = 5\times10^4$, $T_{in} = 633$ K, $P = 24$ MPa.

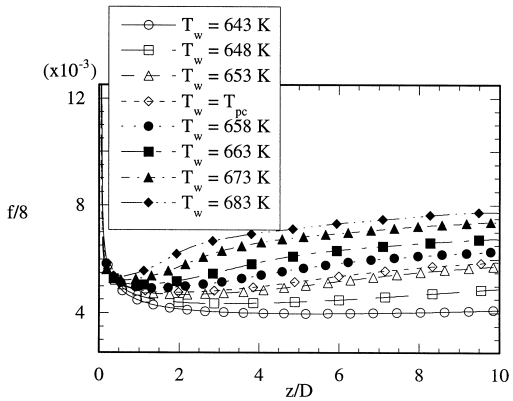

Fig. 10. Friction factor distributions along a tube in upward flow of water for various wall temperatures; $Re = 5\times10^4$, $T_{in} = 633$ K, $P = 24$ MPa.

the wall and the inlet condition. Hence the increase of heat transfer coefficient with wall temperature means an increase in the wall heat flux, caused by the high fluid temperature gradient at the wall.

When the wall temperature is set to the pseudocritical temperature, the fluid specific heat is at a maximum at the wall and thermal conductivity also has a small peak value. Because of the combination of high specific heat and thermal conductivity, the results show that the buoyancy force is very important to flow in a gravity field with heat transfer. Due to the high temperature gradient near the wall the region of high thermal conductivity and specific heat is confined narrowly near the wall. The high diffusion and convection properties at the pseudocritical temperature do not have an important effect on the heat transfer or on momentum transfer in the tube. When the wall temperature is 683 K, the heat transfer coefficient is lower than at 673 K. This is due to the lower wall heat flux which results from lower thermal conductivity, although the buoyancy force is higher.

Figure 10 shows friction factor distributions along the tube, based on the inlet condition. Friction factor also depends on the wall temperature like the heat transfer coefficient. Including the effect of buoyancy, the friction factor increases after some distance from the entrance that depends on the wall temperature. The axial position where the friction factor starts to increase is nearer the entrance ($z/D < 1$ for all wall temperature conditions) compared with the heat transfer coefficient distribution. This shows that the buoyancy effect is a greater factor in momentum transfer than in heat transfer, although they are interconnected. They buoyancy effect produces a high velocity gradient near the wall. This results in a high friction factor even though the viscosity decreases with the increase of temperature.

4.4. Local heat transfer deterioration

In upward flow, turbulent transport is improved due to fluid acceleration by the buoyancy force near the wall. However this acceleration results in an M-shaped radial profile of axial velocity to satisfy mass conservation, and turbulent transport is suppressed due to the decrease of turbulent viscosity [16]. This affects heat transfer and temperature distributions in the tube.

Axial temperature distributions along the tube for several radial positions in upward flow are shown in Fig. 11. Far from the wall or close to the wall, temperature increases continuously along the tube with heat transfer from the wall. At some radial positions, however, temperature first increases, then decreases slightly, and then increases again along the tube. In flow without gravity forces included in the equations, this phenomenon is not observed. It is apparently due to a local decrease of turbulent viscosity combined with radial transport of fluid

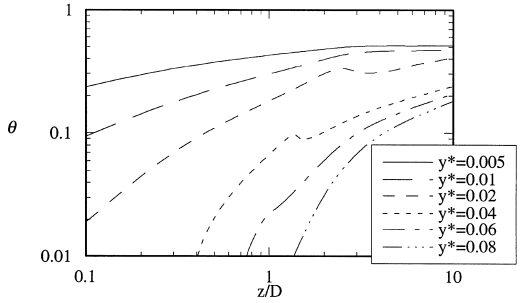

Fig. 11. Axial temperature distributions along a tube in upward flow of water for various radial positions; $Re = 5\times10^4$, $T_{in} = 633$ K, $T_w = 673$ K, $P = 24$ MPa.

from the colder fluid core. Figure 12 shows axial turbulent viscosity and radial velocity distributions for a radial location. At positions corresponding to an axial temperature decrease along the tube, turbulent viscosity values are low and radial velocity is high in the positive direction. A local decrease of turbulent viscosity makes convection important to the heat transfer, and an increase of radial velocity to a locally positive value results in moving of cool fluid from the core of the flow toward the wall. These factors affect and apparently can reverse the axial temperature gradient even though the magnitude of the radial velocity is small.

4.5. Turbulent Prandtl number model

Most of the theoretical and numerical studies of near-critical fluids use 0.9 or 1.0 for turbulent Prandtl number as in the constant property case because there is little information about the effect of property variations. The effect of turbulent Prandtl number model on the differences in predictions from these studies and experimental data are not well explained [29]. In the constant property case, near the wall the turbulent Prandtl number is higher than 1 and far from this region it is almost constant. The varying turbulent Prandtl number near the wall might result in different predictions from those obtained using constant values of 0.9 or 1.0. It is useful to investigate how different predicted results can be obtained by using various models of turbulent Prandtl number, including constant values and varying functions. If the effects of using differing models are small for near-critical conditions, then attention can be directed to other factors.

We investigated the effect of several turbulent Prandtl number models on heat transfer near the critical point. The models and their corresponding figure labels are:

Pr_t: 0.9 (a)

1.0 (b)

$2.0/Pe_t + 0.85$ (c)

$$\frac{1}{\left\{\frac{1}{1.7}+(0.3Pe_t)\sqrt{\frac{1}{0.85}}-(0.3Pe_t)^2\times\left[1-\exp\left(-\frac{1}{\sqrt{0.85}(0.3Pe_t)}\right)\right]\right\}} \quad \text{(d)}.$$

The distributions or Pr_t are shown in Fig. 13 for upward and without-gravity flows. For both flows, Pr_t values near the wall for Kays' model [24] were higher than for other models. It results in lower turbulent heat transport. For upward flow, Pr_t from models (c) and (d) is lower than for flow without gravity because of the larger turbulent eddy diffusivity caused by fluid acceleration. The Pr_t of Kays and Crawford's model [23] approaches 0.9 far from the wall. For flow without gravity, this model predicts a small peak in the region near the wall where there are large property variations. For upward flow, this peak does not appear. This is due to the large increase of turbulent eddy diffusivity from the wall compared with property variations (Prandtl number). For upward flow, turbulent eddy diffusivity increases faster so that the property variation effect on Pr_t is small.

The predicted distributions of heat transfer coefficient and friction factor for the four different turbulent Prandtl numbers are shown in Figs 14 and 15 for upward and without-gravity flows. Because of acceleration near the wall due to the buoyancy effect, the heat transfer coefficient for upward flow is higher than that for flow without gravity. The heat transfer coefficient for $Pr_t = 0.9$ is higher than that for $Pr_t = 1.0$ and $Pr_t = 2.0/Pe_t + 0.85$, and the differences between the heat transfer coefficients using these turbulent Prandtl numbers do not vary significantly along the tube for either flow condition ($z/D > 2$). There is not much difference in heat transfer coefficient along the tube between $Pr_t = 1.0$ and the variation model (d) of Kays and Crawford [23] except near the entrance ($z/D < 2$). At $z/D = 5$, the heat transfer coefficients calculated using $Pr_t = 1.0$ and Pr_t-

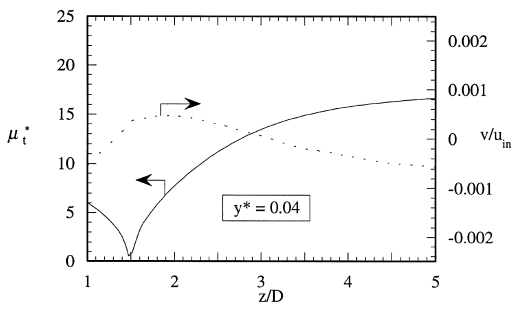

Fig. 12. Turbulent viscosity and radial velocity distributions along a tube in upward flow of water; $Re = 5 \times 10^4$, $T_{in} = 633$ K, $T_w = 673$ K, $P = 24$ MPa.

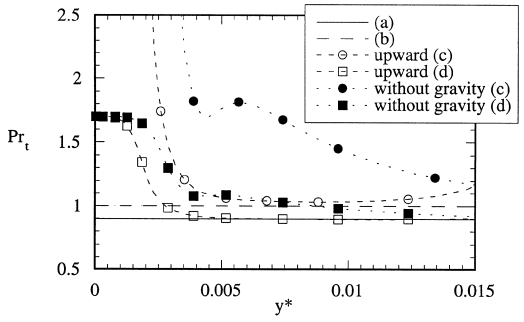

Fig. 13. Turbulent Prandtl number distributions in water for various models; $Re = 5 \times 10^4$, $T_{in} = 633$ K, $T_w = 673$ K, $P = 24$ MPa.

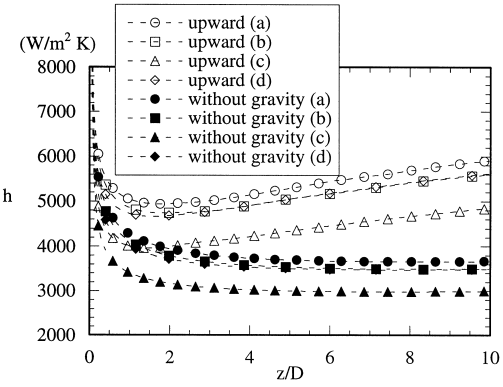

Fig. 14. Comparison of heat transfer coefficient distributions along a tube for various turbulent Prandtl number models for water; $Re = 5\times10^4$, $T_{in} = 633$ K, $T_w = 673$ K, $P = 24$ MPa.

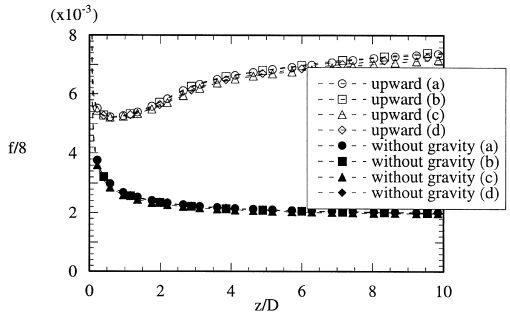

Fig. 15. Comparison of friction factor distributions along a tube for various turbulent Prandtl number models for water; $Re = 5\times10^4$, $T_{in} = 633$ K, $T_w = 673$ K, $P = 24$ MPa.

$= 2.0/Pe_t + 0.85$ are about 4.5 and 17.9% lower than for $Pr_t = 0.9$ for upward flow, while they are about 4.3 and 18.8% lower for flow without gravity.

Near the wall (in the thermal boundary layer), the ratio of turbulent viscosity to molecular viscosity is small. This results in high turbulent Prandtl number in the case of $Pr_t = 2.0/Pe_t + 0.85$, although far from the wall the ratio is large enough to make the term $(2.0/Pe_t)$ very small. As heat transfer is determined in this narrow region of the thermal boundary layer, the heat transfer coefficient for $Pr_t = 2.0/Pe_t + 0.85$ is lower than for $Pr_t = 0.9$ or $Pr_t = 1.0$. The friction factor is essentially unaffected by the differences in the turbulent Prandtl number models; the heat transfer coefficient is.

Although all of the effects are coupled, the results for friction factor show that the changes in the thermal boundary layer do not greatly affect the velocity distributions near the wall. There is at present no experimental data to determine which value of Pr_t produces the best results. These numerical predictions serve to show the effects of common models for Pr_t on the magnitude of h and f. The coupling of property variations makes little difference in friction factor predictions, so any model is adequate; however, care will have to be taken in the choice of model for heat transfer/temperature distribution predictions. This observation may guide experimentalists toward making careful temperature distribution measurements for near-critical conditions so that the choice of model can be made.

5. Conclusions

Turbulent convection heat transfer near the entrance of a vertical tube is numerically investigated for water near the critical point. A modified mixing length model including the effect of density fluctuations is used for turbulent diffusivity. Thermodynamic and transport property variations as strong functions of both temperature and pressure in the flow field affects momentum and heat transport phenomena in the tube. When near the critical pressure, fluid near the wall undergoes larger acceleration due to buoyancy forces and the effect of viscosity variation. Especially steep variations of fluid density near the pseudocritical temperature result in high buoyancy forces, which are important even at large Reynolds number. This flow acceleration increases the heat transfer coefficient near the pseudocritical temperature.

As the wall temperature increases for the same inlet fluid condition, the heat transfer coefficient and friction factor reach a minimum after some distance from the entrance. The friction factor minimum is closer to the entrance.

Local axial decreases in fluid temperature with tube axial position are predicted to occur close to the wall in upward flow. This phenomenon is related to suppressed turbulent transport due to a local decrease of turbulent eddy viscosity and radial convection of cooler tube-core region fluid toward the wall.

Calculations are carried out for several models of turbulent Prandtl number. Comparison of radial distributions in turbulent Prandtl number shows that for variable Prandtl number models, turbulent Prandtl number near the wall for upward flow is lower than for flow without consideration of the gravity force due to the increase of turbulent eddy diffusivity by flow acceleration. This has a large effect on the heat transfer coefficient distribution along the tube for both upward and without-gravity flows, and a negligible effect on friction factor.

References

[1] R.G. Deissler, Heat transfer and fluid friction for fully developed turbulent flow of air and supercritical water with

variable fluid properties, Transactions of ASME 76 (1954) 73–85.
[2] K. Goldman, Heat transfer to supercritical water and other fluids with temperature dependent properties, Chem. Eng. Prog. Symposium 50 (11) (1954) 105–113.
[3] M.E. Shitsman, Temperature conditions in tubes at supercritical pressures, Teploenergetika 15 (1968) 57–61.
[4] B.S. Shiralkar, P. Griffith, Deterioration in heat transfer to fluids at supercritical pressure and high heat fluxes, Journal of Heat Transfer 91 (1) (1969) 27–36.
[5] R.H. Sabersky, E.G. Hauptmann, Forced convection heat transfer to carbon dioxide near the critical point, International Journal of Heat and Mass Transfer 10 (1967) 1499–1508.
[6] R.C. Hendricks, R.J. Simoneau, R.V. Smith, Survey of heat transfer to near critical fluids, NASA Technical Note, 1970, NASA TN D–5886.
[7] W.B. Hall, Heat transfer near the critical point, Advances in Heat Transfer 7 (1971) 1–83.
[8] J.D. Jackson, W.B. Hall, Forced convection heat transfer to fluids at supercritical pressure, Turbulent Forced Convection in Channels and Bundles, Hemisphere, New York, 1979, pp. 563–611.
[9] B.S. Petukhov, N.V. Medvetskaya, Turbulent flow and heat transfer in heated tubes for single phase heat careers with near critical parameters, Teplofizika Vysokikh Temperature 17 (2) (1979) 343–350.
[10] A.J. Ghajar, A. Asadi, Improved forced convective heat transfer correlations for liquids in the near critical region, AIAA Journal 24 (1986) 2031–2037.
[11] A.F. Polyakov, Heat transfer under supercritical pressures, Advances in Heat Transfer 21 (1991) 1–50.
[12] V.A. Kurganov, A.G. Kaptilnyi, Flow structure and turbulent transport of a supercritical pressure fluid in a vertical heated tube under the conditions of mixed convection experimental data, International Journal of Heat and Mass Transfer 36 (1993) 3383–3392.
[13] N.M. Schnurr, Numerical predictions of heat transfer to supercritical helium in turbulent flow through circular tubes, Journal of Heat Transfer 99 (1977) 580–585.
[14] C.P. Bellmore, R.L. Reid, Numerical prediction of wall temperatures for near-critical para-hydrogen in turbulent upflow inside vertical tubes, Journal of Heat Transfer 105 (1983) 536–541.
[15] E.P. Valueva, V.N. Popov, Numerical modeling of mixed turbulent convection of water at subcritical and supercritical pressure, Teploenergetika 32 (1985) 62–65.
[16] U. Renz, R. Bellinghausen, Heat transfer in a vertical pipe at supercritical pressure, Proceedings of the 8th International Heat Transfer Conference 3 (1986) 957–962.
[17] V.N. Popov, E.P. Valueva, Heat transfer and turbulent flow of water at supercritical parameters of state in a vertical tube with a significant effect of free convection, Teploenergetica 33 (1986) 22–29.
[18] S. Koshizuka, N. Takano, Y. Oka, Numerical analysis of deterioration phenomena in heat transfer to supercritical water, International Journal of Heat and Mass Transfer 38 (1995) 3077–3084.
[19] N. Zhou, A. Krishnan, Laminar and turbulent heat transfer in flow of supercritical CO_2, Proceedings of the 30th ASME National Heat Transfer Conference, Portland 5 (1995) 53–63.
[20] S.H. Lee, J.R. Howell, Laminar forced convection at zero-gravity to water near the critical region, Journal of Thermophysics and Heat Transfer 10 (1996) 504–510.
[21] S.H. Lee, J.R. Howell, Gravitational effects on laminar forced convection heat transfer in a vertical tube for water near the critical region, Journal of Thermophysics and Heat Transfer 10 (1996) 627–632.
[22] S.H. Lee, J.R. Howell, Turbulent developing convective heat transfer in a tube for fluids near the critical point, Int. J. Heat Mass Transfer 41 (10) (1998) 1205–1218.
[23] W.M. Kays, M.E. Crawford, Convective Heat and Mass Transfer, McGraw-Hill, 1993.
[24] W.M. Kays, Turbulent Prandtl number—where are we?, Journal of Heat Transfer 116 (1994) 284–295.
[25] H. Lester, S.G. John, S.K. George, Steam Tables, Hemisphere, New York, 1984.
[26] S.V. Patankar, Numerical Heat Transfer and Fluid Flow, Hemisphere, Washington, DC, 1980.
[27] D.A. Anderson, J.C. Tannehill, R.H. Fletcher, Computational Fluid Mechanics and Heat Transfer, McGraw-Hill, 1984.
[28] R.C. Hendricks, A.K. Baron, J.C. Peller, GASP-A computer code for calculating the thermodynamics and transport properties for ten fluids, NASA Technical Note, 1975, NASA TN D-7808.
[29] A.J. Reynolds, The prediction of turbulent Prandtl and Schmidt numbers, International Journal of Heat and Mass Transfer 18 (1975) 1055–1069.